Transient CHF enhancement in high pressure pool boiling on rough surface

Avdhoot Walunj*, A. Sathyabhama

Department of Mechanical Engineering, National Institute of Technology Karnataka, Surathkal, 575025, India

ARTICLE INFO

ABSTRACT

Experimental investigation of transient pool boiling heat transfer (PBHT) to saturated water from thick, non-lumped 20 mm diameter copper sample is carried at 1 bar, 5 bar and 10 bar pressure. The time constant (γ) of exponential heat supply is varied from 1 to 6. The unidirectional scratches are made on the surface to obtain wide range of surface roughness varying from $R_a = 0.106\,\mu m$ to $R_a = 4.03\,\mu m$. The effect of surface roughness, pressure and time constant on transient critical heat flux (CHF) is extensively studied. Transient CHF enhancement for $R_a = 4.03\,\mu m$ when $\gamma = 1$ is found to be 98.88%, 76.55% and 53.21% at pressures P = 1 bar, P = 5 bar and P = 10 bar, respectively, however it is found to be lower by 9.38%, 21.40% and 9.73%, compared to steady state CHF enhancement for $R_a = 4.03\,\mu m$, at respective pressures. The Gorenflo correlation is modified by including the additional parameter γ and it predicts the present transient HTC values with mean absolute error (MAE) of 14.91%. The CHF model is developed by considering the effect of capillary wicking in the narrow unidirectional scratches and the bubble angle. This model predicts the present transient CHF values with MAE of 11.89%.

1. Introduction

The heat generation in the nuclear reactor is directly proportional to the exponential of time constant ($Q \propto e^{\gamma}$) where $\gamma = t/\tau$, t is the period of heating (sec) and τ is the exponential period (sec). Such exponential power excursion in the bulky and non-lumped mass of nuclear fuel rod may lead to the meltdown of the components due to loss of coolant. The heat generation in the nuclear reactor should be efficiently removed by the boiling fluid to keep the system temperature under control. It is important to understand the transition mechanism of the non-boiling to the film boiling regime of the fluid on thick heater. The experimental investigation of the transient pool boiling heat transfer (PBHT) from thin elements like ribbon, cylinder, wire or film during different transient heat supply like pulse, exponential or linear step type of heating is carried out by the researchers and summary is presented in Table 1. The transient CHF enhancement by surface modification of thin elements is also reported by few researchers. For the first time, Rosenthal [1] examined the effect of transient heating on the transient CHF at atmospheric pressure on platinum ribbon and reported that transient CHF is not influenced by the transient state of heat supply. Johnson [2] investigated the transient boiling heat transfer at pressure up to 13.78 MPa and commented that transient CHF for exponential heat input exceeds the steady-state CHF. Extensive work is carried by Sakurai and his research team [3–5] to understand the transient boiling under exponential heat supply using thin elements on different wetting

fluids at different pressures. Sakurai et al. [3] studied the non-boiling to film boiling transition in liquid nitrogen on horizontal cylinder for various transient heat supply. They reported that steady state CHF is higher than transient CHF. Sakurai and Shiotsu [4,5] carried experiments on platinum wire in pool of water and reported that incipient boiling temperature and its corresponding heat flux increases with decrease in exponential period. They have found the non-uniform trend of transient HTC with the exponential period. They commented that transient CHF increases initially, then decreases and finally increases as the exponential period decreases. Deev et al. [6] studied the effect of heat generation in a heater on the transition from nucleate to film boiling regime. A drastic reduction in the critical time interval and transient CHF is reported in their study. They commented that transient CHF decreases significantly with increase in the initial heat load. Duluc et al. [7] studied the role of nucleation site density and the thermal inertia of the flat thick test piece during stepwise heat generation. They observed that onset of nucleate boiling (ONB) temperature in steady-state condition is lower than that in stepwise heating. Recently, Su et al. [8] studied boiling crisis on a plate heater due to exponential heating. They identified ONB, onset of the boiling driven (OBD) phase and temperature overshoot conditions for different period of exponential transient. The ONB temperature and corresponding heat flux is found to be increased with increase in the rate of exponential heating. Balakin et al. [9] studied the influence of pressure, heater size and type of the fluid on the boiling crisis during unsteady heating. They commented

Nomenclature

C	constant
C_p	specific heat (J/kg K)
D_b	diameter of bubble (m)
F	force (N)
g	gravity (m/s^2)
H_b	bubble height (m)
h	heat transfer coefficient (W/m^{2}K)
h_{fg}	latent heat (J/kg)
k_{cu}	thermal conductivity of copper (W/mK)
m	exponent for surface roughness
N	number of capillary tubes
n	exponent for heat flux
P	pressure (bar)
P_r	reduced pressure
Pr	prandtl number
Q	heat input (W)
q''	heat Flux (W/m^2)
R_a	average roughness (μm)
R_q	root mean squared roughness (μm)
R_z	ten-point average roughness (μm)
S_m	mean spacing (μm)
T	temperature (°C)
t	time (sec)
x	distance (mm)

Greek Symbols

ΔT	wall superheat (°C)
γ	time constant
τ	exponential period (sec)
Θ	angle (°)
λT	Taylor unstable wavelength (m)
μ	viscosity (N s/m^2)

ρ	density (kg/m^3)
σ	surface tension (N/m)

Subscripts

b	bubble
0	reference
c	capillary
g	gravity
l	liquid
m	momentum
ov	overshoot
s	surface tension
sat	saturated
suf	surface
ss	steady-state
ts	transient-state
v	vapor
w	wall

Abbreviations

CHF	critical heat flux
CS	commercial surface
HI	hydrodynamic instability
HSN	heterogeneous spontaneous nucleation
HTC	heat transfer coefficient
MAE	mean absolute error
MS	mirror surface
OBD	onset of boiling driven
ONB	onset of nucleate boiling
OV	overshoot
PBHT	pool boiling heat transfer
RS	rough surface

that size of the heater highly influences the extremum boiling crisis. Drach et al. [10] studied the effect of surface roughness on the transient PBHT of liquid nitrogen. A wide range of surface roughness values from $R_a = 0.1$ μm to 4.8 μm was examined. The researchers reported that the ONB temperature exponentially drops with an increase in the surface roughness value. However, they also observed that the increase in transient CHF with the R_a was lower than the steady state CHF for all the transient heat inputs. Fukuda et al. [11] also investigated the effect of surface conditions of platinum cylinders in a pool of water on the two different surface conditions with mirror surface (MS) and a rough surface (RS) finished, however the exact surface roughness values are not reported. Marginal changes are observed in transient boiling heat transfer due to RS. Park et al. [12] investigated the dynamic PBHT of highly wetting fluid like FC-72 from 1 mm diameter horizontal cylinder under an exponential heat supply. Two distinct mechanisms viz. HI, and HSN were reported. The CHF in the steady-state condition at lower subcooling occurred due to the time lag of HI, whereas the explosive process of HSN during short period of transient in originally flooded cavities resulted in the transient CHF. A comparative heat transfer study was done between commercial surface (CS) of $R_a = 0.11$ μm and RS of $R_a = 0.24$ μm. The CHF of the CS was considerably lower than that of the RS during the short period, whereas it suddenly increased with the increase in the period. This means that CHF during a short period is highly influenced by the surface roughness. Htet et al. [13] experimentally tested the transient boiling characteristics on CS, treated surface I (TS-I) polished by buff paper together with alumina and treated surface II (TS-II) finished by emery paper of a vertically oriented ribbon. During slow transient, the enhancement in transient CHF of TS-

II was found to be 16% and 28% compared to the CS and the TS-I, respectively. They also reported that transient CHF are dependent on the period of transient as well as system pressure. It can be concluded from the literature that most of the transient pool boiling study is carried out with a lumped test sample like wire, thin cylinder or ribbon. The effect of exponential transients on the transient heat flux from the thick, non-lumped sample is rarely studied. The surface modification for the heat transfer enhancement in water during transient heating is rarely done. A unified correlation of HTC and CHF model for rough surface during exponential heat supply is also not yet developed.

In the present study, the transient boiling characteristics of saturated water under high pressure on thick rough sample are investigated. The effect of exponential heat supply with different time constant and pressure on ONB and CHF is studied. The enhancement in transient CHF due to surface roughness is also reported. The compound effect of surface roughness and rate of exponential heat supply on HTC is examined. A correlation, which predicts non-dimensional h_{ts} is developed from the non-dimensional independent parameters- P_r, γ, R_a and q''_{ts}. A CHF model is developed by considering capillary wicking and contact angle.

2. Experimentation

2.1. Preparation of test samples

The top surface of six samples is polished by the 2000 grit sandpaper to remove the contamination and to obtain uniform surface finishing. Later, the test surface is polished by 1200, 800, 600, 120, 80, and 60

Table 1
Summary of the experimental conditions used in the literature.

Authors	Medium	Heating Element	Element Material	Period/rate of exponential transients	Subcooling	Operating Pressure	Surface condition	Camera (fps)
Rosenthal [1]	Water	Ribbon (0.025 mm thick, 2.5 mm wide)	Platinum and Aluminium	Exponential (τ = 5–75 ms)	0–68 K	Atmospheric	–	6000
Johnson [2]	Water	Ribbon 0.10/0.36 mm thick 3.2 mm wide	Platinum	Exponential (τ = 5 to 50 ms)	5–62 K	Ambient to 13.8 MPa	–	–
Sakurai et al. [3]	LN_2	Cylinder (φ = 1.2 mm)	Platinum	Exponential (τ = 7 ms- 100 s), Stepwise	0–77.4 K	Atmospheric-2.047 MPa	–	200
Sakurai and Shiotsu [4,5]	Water	wire (φ = 1.2 mm)	Platinum	Exponential (τ = 5 ms- 10 s)	25–75 K	Atmospheric	–	–
Deev et al. [6]	Water	Wire (Φ = 0.1 mm)	Platinum	Stepwise	Saturated	Atmospheric	–	–
Duluc et al. [7]	LN_2	Thick sample (Φ = 30 mm), Wire (Φ = 25 μm)	Copper Bronze	Stepwise	Saturated	Atmospheric	R_a = 0.06 μm and R_a = 1 μm	–
Su et al. [8]	Water	0.7 μm thick film	ITO/sapphire	Exponential (τ = 5 ms-500 ms)	0–75	Atmospheric	–	5000
Balakin et al. [9]	LN_2	Wire (Φ = 100μm)	Platinum	Pulse	–	0.1-0.4 MPa	–	–
Drach et al. [10]	LN_2	Film	Ni And Varnish (SiO_2)	Pulse (~0.25 s)	–	Atmospheric	R_a = 0.1,1.4, 2.4, 3.6,4.8 μm	–
Fukuda et al. [11]	DI Water	Cylinder (Φ = 1.2mm)	Platinum	Exponential (τ = 2 ms–20s)	0–60 K	Atmospheric-1.082 MPa	CS (R_a = 0.11 μm) and RS (R_a = 0.24 μm)	1000
Park et al. [12]	Ethanol and FC-72	Cylinder (Φ = 1 mm)	Platinum	Exponential (τ = 20 ms-2s)	0–60 K	Atmospheric-1.082 MPa	CS (R_a = 0.11 μm) and RS (R_a = 0.24 μm)	1000
Htet et al. [13]	Water	Ribbon 0.05 mm–0.1 mm thick	Platinum	Exponential (τ = 5 ms-20 ms)	0–20 K	0.1–0.297 MPa	R_a = 0.04 μm, R_a = 0.12 μm, R_a = 0.22 μm	–

grit sandpaper in a single direction which forms the unidirectional scratches. The number of stroke during the polishing is gradually increased from 5 for 60 grit sandpaper to 50 for 1200 grit sandpaper. Uniform pressure and continuous distilled water supply on the polishing surface are maintained during sample preparation. After polishing, all samples are sequentially cleaned in acetone, ethanol, and distilled water.

2.2. Characterization

The samples are characterized by roughness and wettability measurement in two steps, namely, before and after the boiling test. The roughness parameter is measured using roughness tester (Mitutoyo). Each sample is tested at six different locations where unidirectional scratches are perpendicular to the direction of the testing probe. The evaluation length is 4 mm. The uniformity of the roughness values is ensured over the entire surface by permitting ± 0.1 μm variation in the readings of six different locations. The static contact angle of the 10 μl water droplet for each sample is measured using goniometer (GBX Digidrop). The contact angle is measured by positioning the unidirectional scratches parallel and perpendicular to the axis of the camera.

2.3. Experimental setup

The experimental setup, as shown in Fig. 1, mainly includes a boiling chamber, test section, condenser unit, and CCD camera. The rectangular chamber has removable top and bottom flanges. The condenser coil is connected with the pump and is fixed to the top flange. The test section is fitted to bottom flange. A K-type thermocouple and a pressure transducer are fixed to the boiling chamber to measure the bulk fluid temperature (T_l) and chamber pressure, respectively. Auxiliary heaters of 2000 W capacity are used to maintain the saturated condition of the distilled water. Transparent borosilicate glass is provided to the wall of boiling chamber for the visualization study. The setup is integrated with NI-9213 temperature module and NI-9264 to acquire temperature readings and to interface the computer with power supply, respectively.

2.4. Test section

20 mm diameter and 20 mm length copper samples are prepared and characterized. The main heater is inserted in the heating block. Though the sample can be fixed on the heating block with perfect surface contact, thin layer of thermal paste is applied to eliminate the air gap. The assembly of sample and heating block is perfectly insulated with glass wool bed as shown in Fig. 2. Glass wool bed is covered with thick Teflon block. An O-ring and high-temperature non-corrosive RTV silicone gasket are used between the test sample and insulation block to prevent leakage and to avoid edge effect during the boiling test. K-type sheathed thermocouples of 1 mm diameter are used to measure the temperature of the test sample at different locations. The thermocouples are implanted at 2 mm, 6 mm, and 10 mm in the test sample from the top surface and the temperatures T_{m-1}, T_m, and T_{m+1} correspond to these thermocouple readings, respectively.

2.5. Experimental procedure

The known quantity of DI water is filled in the boiling chamber during each trial. DI water is rigorously boiled before each trial by the auxiliary heater to remove the dissolved gases. Controlled analog signals are generated through NI-9264 which is monitored by LABVIEW program. Thus exponentially varying voltage controlled-current signals are supplied to the main heaters through the programmable DC power supply (Sorensen; XG series). The time-variant exponential heat is supplied where time constant varies from $\gamma = 1$ to $\gamma = 6$. The period of exponential transient (t) is 10 min. The time constant is calculated as
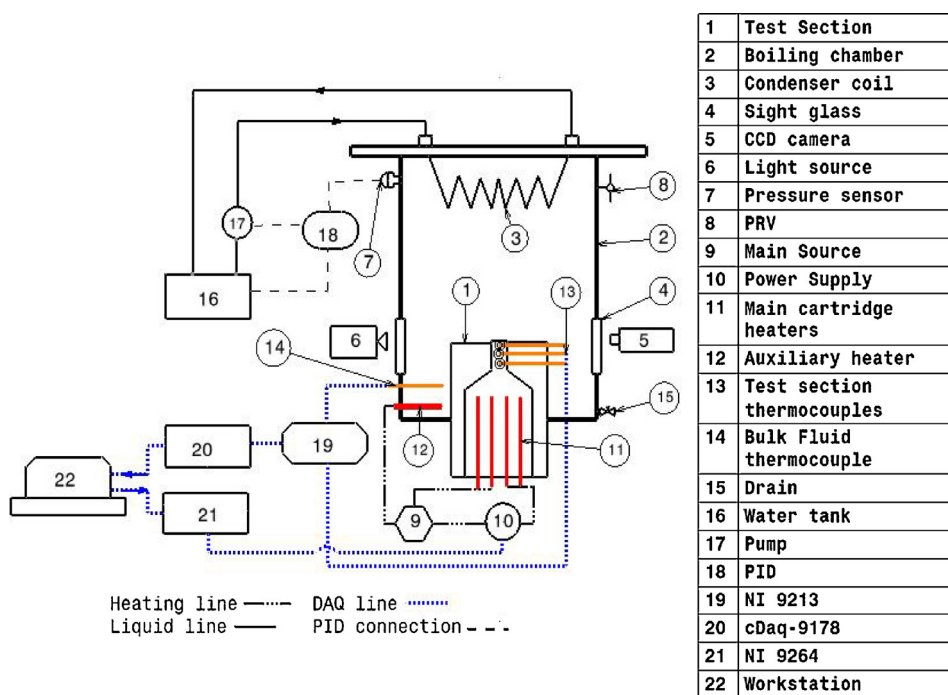
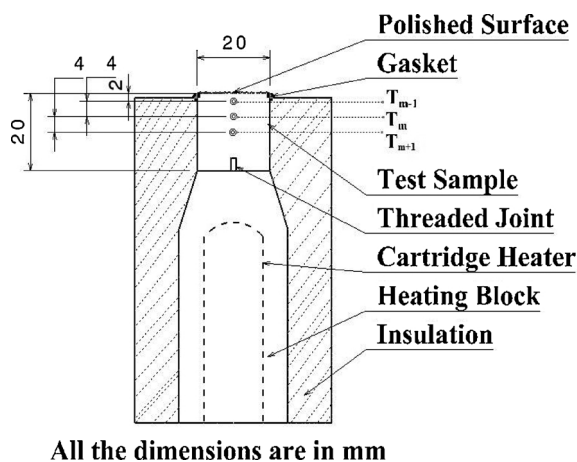| 1	Test Section
2	Boiling chamber
3	Condenser coil
4	Sight glass
5	CCD camera
6	Light source
7	Pressure sensor
8	PRV
9	Main Source
10	Power Supply
11	Main cartridge heaters
12	Auxiliary heater
13	Test section thermocouples
14	Bulk Fluid thermocouple
15	Drain
16	Water tank
17	Pump
18	PID
19	NI 9213
20	cDaq-9178
21	NI 9264
22	Workstation

Fig. 1. Experimental Setup.

Fig. 2. Test Section.

Fig. 3. Temperature distribution along the length of the sample.

$\gamma = t/\tau$ where τ is exponential period. The LABVIEW program is also designed for recording the temperatures of the test piece at an acquisition rate of 5 samples/sec by a NI-9213 temperature module through cDaq-9178. The high speed camera (AOS Promon 501) used to record boiling phases at certain interval of time is placed in front of the sight glass. Diffused light source is placed in front of opposite sight glass. The camera can record video at 1000 frames/s with 480 × 240 pixel resolution. AF NIKKOR 50 mm F/1.4D lens is used. The heat supply, temperature acquisition and the high speed camera are synchronized through workstation. The pressure in the chamber is controlled by a proportional integral derivative (PID) pressure controller. Pressure transducer synchronized with PID permits ± 0.01 bar pressure variation during the trial.

The main heater and test sample are considered as the axisymmetric system. As the surface properties are found to be uniform during characterization, the heat flux from the top surface of the test sample is assumed to be uniform. The heat flux dissipated to the boiling fluid and the surface temperature can be estimated by the thermocouple readings. The temperature distribution along the length of the test sample of
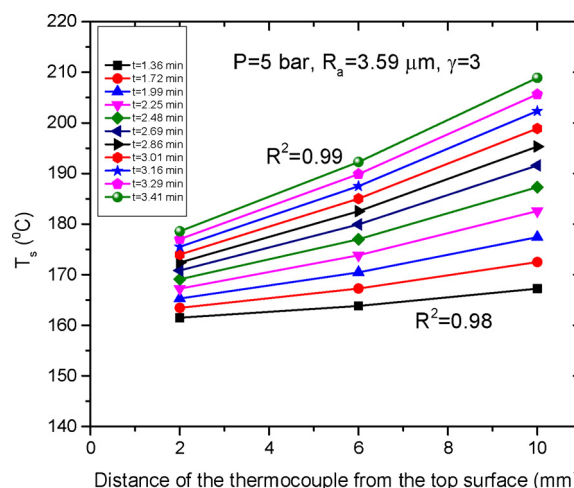
$R_a = 3.59\,\mu m$ at P = 5 bar and $\gamma = 3$, shown in Fig. 3, is obtained by thermocouples which are implanted at 2 mm, 6 mm and 10 mm from the boiling surface. Though the temperature distribution at all the time intervals are not perfectly linear ($R^2 \neq 1$), a linear fit is established. This non-linearity exists due to temperature maldistribution close to boiling surface during nucleate boiling. Gong and Cheng [14] investigated such temperature maldistribution based on pseudo-potential liquid-vapor phase change lattice Boltzmann model. They found that the depth of penetration of such maldistribution during transition regime is three times the capillary length. The isotherm located in this depth does not appear straight horizontal indicating non-uniform temperature distribution. In the present study, temperature measurement by the thermocouple implanted at 2 mm from the boiling surface may get affected due to significant maldistribution during high pressure nucleate boiling.

The unsteady state heat flux from the top surface of the sample due to exponential heating is calculated by Eq. (1).

$$q_{ts}'' = -k_{Cu}\frac{T_{m-1}^t - T_{m+1}^t}{2\Delta x} \tag{1}$$

where Δx is the distance between two thermocouples.

The surface temperature of the sample is calculated by using Eq. (2).

$$T_w^t = T_{m-1}^t - q_{ts}''\left(\frac{x_{m-1}}{k_{Cu}}\right) \tag{2}$$

where, x_{m-1} is the distance between the surface of a sample and a top thermocouple (T_{m-1}) and is equal to 2 mm, as shown in Fig. 2.

Heat transfer coefficient (HTC) between the surface and water is estimated by Eq. (3).

$$h_{ts} = \frac{q_{ts}''}{(T_w^t - T_l)} \tag{3}$$

2.6. Uncertainty

The uncertainty calculations are done by propagation of error method. Due to temperature maldistribution, the uncertainty in the temperature (T_{m-1}^t) measurement is $\pm$ 1.1 °C. The uncertainty in temperature (T_{m+1}^t) and distance measurement is $\pm$ 0.1 °C and $\pm$ 0.0001 m, respectively. At high temperature, the uncertainty in the heat flux is found to be 11.91% while the uncertainty in the surface temperature is $\pm$ 0.55 °C. The uncertainty in the HTC is found to be 16.20% at a higher operating temperature. The uncertainty in the contact angle measurement is $\pm$ 1°. The uncertainty in pressure measurement is 0.2% (full span is 0–27.4 bar).

3. Result and discussion

The average of roughness parameter obtained before and after boiling test is tabulated in Table 2. R_a is estimated by considering the average length between the peaks and valleys and the deviation from the mean line on the entire surface within the sampling length. Thus R_a neutralize the extreme peak or valley. R_z, the absolute depth of the scratch, is the average of only five highest peak and five deepest valley within sampling length. Furthermore, the wavelength of the scratches that can be called as mean spacing between capillary tubes (S_m), is also measured. It is clear and also confirmed in the literature [15,16] that R_a fails to distinguish between two surfaces of different topography. On the other hand, though R_z accounts TO the peak-to-valley distance, the considered samples are just five. Thus to characterize the large flat surface, R_z does not fit as a better measure. In the present study unidirectional scratches are made on the sample where each scratch is assumed as a capillary tube. Thus equivalence between radius of the tube and R_a is considered. Further the number of capillary tubes can be related to the mean spacing S_m. Thus R_a and S_m is taken into account and its combined role in pool boiling heat transfer is discussed in the present study where term R_a is used for classification of the tested samples. This assumption seems most suitable than considering R_z. Though R_a and S_m is considered as roughness parameter in this study, role of R_z in the pool boiling heat transfer can not be neglected. The static contact angle is measured at different sample position viz. perpendicular and parallel to the axis of camera. The average of four measured contact angles corresponding to each sample is considered in the present study, as shown in Fig. 4.

3.1. Typical boiling processes

The repeatability of the experimental values are verified by the three pre-experimental runs on the plain surface. The validation of the experimental results is presented in Walunj and Sathyabhama [17]. Thereafter, boiling curves for rough surfaces at different pressure are obtained from single trial.

3.1.1. State of heating

The systematic study is carried out to examine the changes in the boiling process during exponential heat supply compared to the steady state condition. Fig. 5 shows the boiling curve of the smooth surface of $R_a = 0.106\,\mu m$ for steady and quasi-steady heat supply at P = 1 bar. Steady state study comprises of an incremental heat supply at a certain time interval ensuring the steady state condition of the temperature of the sample. The mechanism of the bubble formation is found to be steady where nucleation sites get activated gradually with increase in the incremental heat supply. The mechanism of the liquid replenishment does not affect adversely and hence the fully developed nucleate boiling (FDNB) regime is found to be prolonged. The boiling phases from non-boiling to the film boiling are carefully noticed during exponential heat supply. Non-boiling phase turns to nucleate boiling at point A' as shown in Fig. 5. Heat flux rapidly changes after point A' due to heterogeneous spontaneous nucleation (HSN) in the originally flooded cavities. This boiling phase is able to extract the heat from the sample surface as efficiently as that of steady state and thus it follows the steady state curve upto point B'. The stored energy in the sample continuously increases due to exponentially increasing heat supply. The entire surface gets covered with the discrete bubble and thus FDNB phase begins at point B'. Rapid increase in the surface temperature leads to an instability in the liquid-vapor motion and thus, liquid supply to the dry-out area becomes inefficient. Bubble coalescence is observed where bubble begins to spread horizontally on the surface. This mechanism of bubble growth degrades the heat dissipation from the surface which results in the increase in surface temperature. Finally, transition into film boiling regime occurs at point C' where vertical and horizontal bubble coalescence forms vapor film on the entire surface. It is commented that the boiling mechanism is influenced by the heating condition.

3.1.2. Transient boiling curve

The transition mechanism in the boiling process of smooth surface during quasi-steady and rapid exponential supply is also studied. The boiling curves of the sample of $R_a = 0.106\,\mu m$ at $\gamma = 1$ and $\gamma = 6$ are shown in Fig. 6. The transition from non-boiling regime to boiling regime substantially depends on the rate of exponential heat supply. For quasi-steady heat supply of $\gamma = 1$ with long period, nucleation occurs at lower wall superheat (point A) compared to that for rapid heat supply of $\gamma = 6$ with short period (point A') as shown in Fig. 6. Spontaneous nucleation occurs at point A resulting in high flux from the surface which turns into FDNB regime at point B. Quasi-steady transition from FDNB regime to film boiling regime is found at point C due to slow exponential heating at large period. As commented by Sakurai et al. [3], during quasi-steady heat supply, HSN occurs at less number of nucleation sites which result in the gradual levitation of the superheated liquid from the boiling surface. Small number of detached bubbles cause mixing of the superheated liquid with the bulk fluid and will activate the remaining originally flooded cavities. This entire process occurs slowly and hence wall superheat increases gradually with the increase in the heat flux. During heat supply at $\gamma = 6$, non-boiling regime, governed by natural convection heat transfer, turns into boiling regime at point A'. At $\gamma = 6$, since rapid heat is supplied for a short period, explosive bubble formation is observed which results in

Table 2
Roughness parameters in μm.

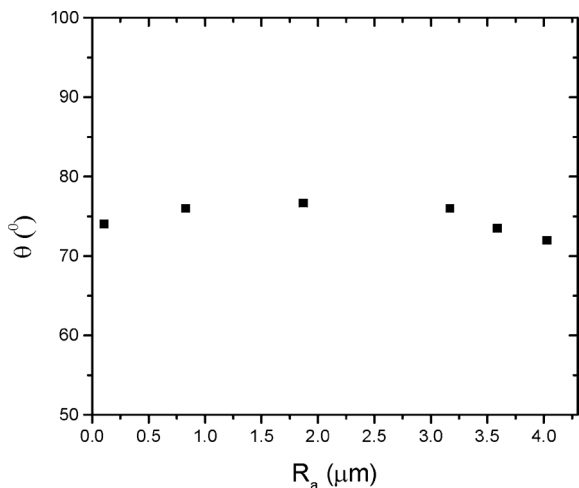| R_a	R_z	R_q	S_m
0.106	1.20	0.14	13.2
0.83	7.05	1.07	26.8
1.87	13.30	2.40	35.7
3.17	22.91	4.12	42.2
3.59	27.55	4.09	44.8
4.03	26.50	4.95	45.2

Fig. 4. Variation in static contact angle with R_a.
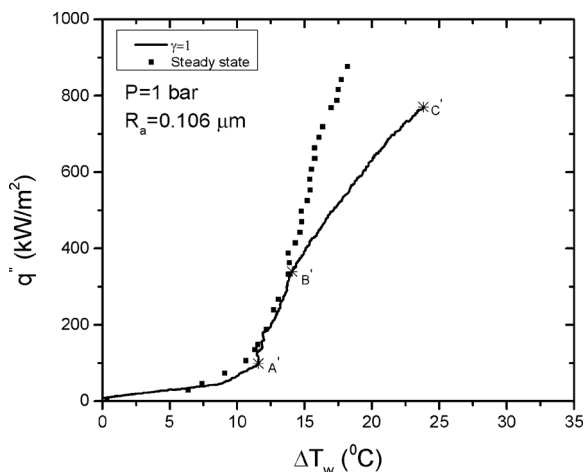

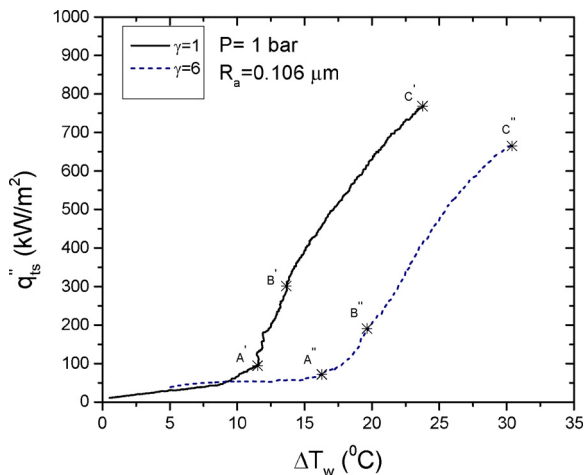**Fig. 5.** Boiling curves at steady and quasi-steady heat supply.

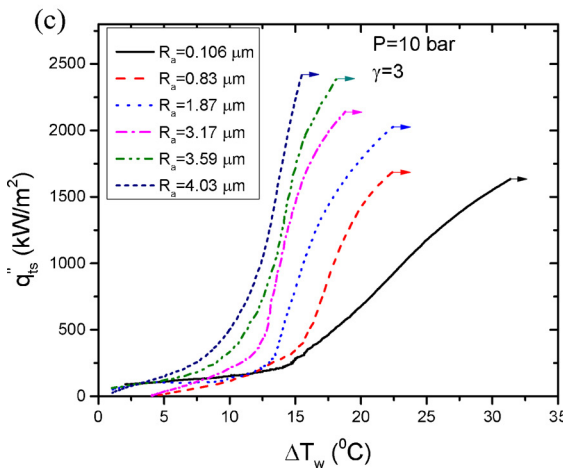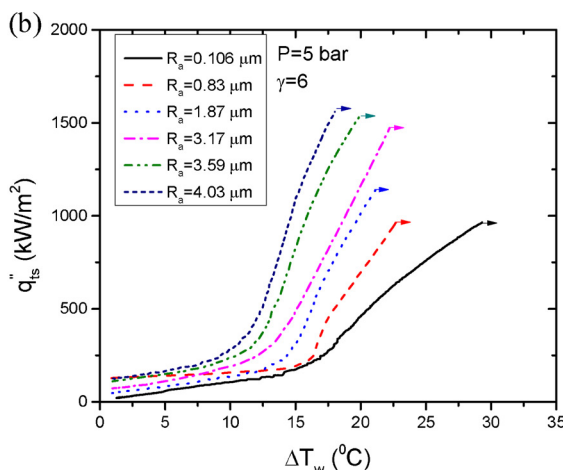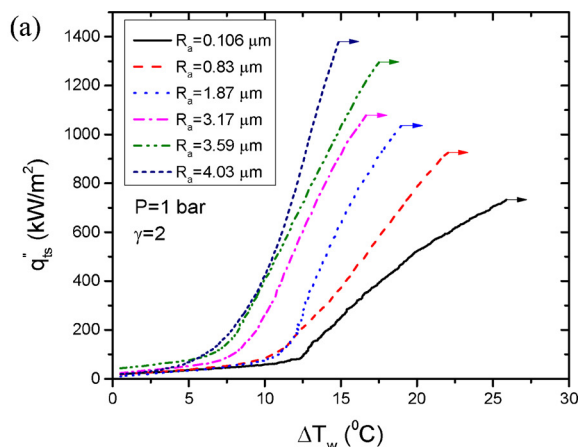**Fig. 6.** Boiling curves at exponential heat supply of $\gamma = 1$ and $\gamma = 6$.

Fig. 7. Effect of surface roughness on transient pool boiling heat transfer at (a) P = 1 bar, $\gamma = 2$ (b) P = 5 bar, $\gamma = 6$ (c) P = 10 bar, $\gamma = 3$.

3.2. Effect of surface roughness on transient pool boiling heat transfer

The trials are conducted with the samples of wide variation in the surface roughness values at 1 bar, 5 bar and 10 bar pressures by supplying exponential heat at different time constant. The representative boiling curves of different R_a are shown in Fig. 7(a)–(c) for P = 1 bar; $\gamma = 2$, P = 5 bar; $\gamma = 3$ and P = 10; $\gamma = 6$, respectively. Program controlled quasi-steady heat ($Q \propto e^\gamma$) is supplied at $\gamma = 1$ for long period of transient whereas rapid heat is supplied at $\gamma = 6$ for short period of transient. It is clearly observed from Fig. 7 that boiling curves of the sample move to the left with increase in R_a indicating increase in heat transfer coefficient due to enhanced heat transfer at reduced wall

the sudden rise in heat flux during boiling phase from A' to B'. Thus semi-direct transition is observed from the FDNB to film boiling regime during rapid heat supply. It is commented that the nature of phase transition from non-boiling to film boiling regime depends on the rate of exponential heat supply.

superheat. The absolute depth R_z plays vital role in boiling incipience. It is observed during characterization that R_z increases with increase in R_a. Thus the cavities on the surface increase resulting in early boiling incipience. It is observed that the ONB temperature gradually decreased with increase in R_a at different pressures. Further, the unidirectional scratches act as narrow passages for the liquid supply to the nucleation sites. Liquid replenishment improved due to capillary action through the scratches. This mechanism enhances the heat transfer. It is found during heat supply of $\gamma = 6$ at $P = 5$ bar that ONB temperature for $R_a = 0.83\,\mu m$, $R_a = 1.87\,\mu m$, $R_a = 3.17\,\mu m$, $R_a = 3.59\,\mu m$ and $R_a = 4.03\,\mu m$ reduced by 4.73%, 12.50%, 26.76%, 34.14% and 38.42%, respectively, from that of $R_a = 0.106\,\mu m$.

3.3. Effect of exponential heat supply on pool boiling

The exponential heat is supplied to the samples of different R_a at time constant γ varying from 1 to 6 at different pressures. Fig. 8(a)–(c) depict the effect of γ on pool boiling heat transfer for selected combination of P and R_a. It is found that time constant γ affects the boiling process adversely irrespective of the surface characteristics and system pressure. Boiling curves plotted in Fig. 8 for each sample shift towards right with increase in γ which suggests that heat transfer decreases with increase in γ. The mechanism of heat transfer gradually becomes unstable due to increase in the rate of heating. The number of complete bubble cycles that can be possible at each nucleation site reduces with increase in the rate of heating. The rapidly increasing heat supply during short period ($\gamma = 6$) triggers the bubble frequency which leads to the early bubble coalescence. The FDNB regime drastically reduces with increase in the rate of heating. It is also noticed that ONB heat flux and ONB temperature increase with increase in the time constant. Similar results are reported by Su et al. [8] and Sakurai et al. [18]. They suggested that the variation in moment of ONB can be estimated by a combination of the analytic transient conduction temperature profile in water and the Hsu's nucleation criterion. It is observed during the trial at $P = 5$ bar on the sample $R_a = 4.03\,\mu m$ that ONB temperature during heat supply at $\gamma = 2$, $\gamma = 3$, $\gamma = 4$, $\gamma = 5$ and $\gamma = 6$ increased by 39.07%, 49.39%, 74.51%, 122.81% and 133.98%, respectively, from that of $\gamma = 1$.

3.4. Effect of pressure on transient pool boiling

The pool boiling tests are conducted at 1, 5 and 10 bar pressures on each sample. It is found that the transient heat transfer from the sample substantially increased with increase in the pressure. Points A, A' and A'' marked on the boiling curves represent the ONB point at $P = 1$ bar, 5 bar and 10 bar, respectively, as shown in Fig. 9, for $\gamma = 1$ and $\gamma = 3$. The ONB temperature reduced with increase in the pressure. Rate of heat transfer immediately after the spontaneous nucleation also increased with increase in the pressure. The partial nucleate boiling regime turns into FDNB regime at point B, B' and B'' where nucleate boiling regime extends with increase in pressure irrespective of the rate of transient. The transition from FDNB regime to film boiling regime varies with the pressure. At $P = 1$ bar and 5 bar, semi-direct transition is noticed at point C and C', respectively, whereas at $P = 10$ bar, quasi-steady transition is noticed at point C''. During visualization, it is found that tiny bubbles are formed and depart independently at high pressure and hence bubble coalescence is retarded resulting in drastic increase in the heat transfer compared to 1 bar and 5 bar pressures. It is commented that heat flux is strong function of system pressure compared to the time constant of exponential heat supply.

3.5. Onset of nucleate boiling and overshoot temperature

In the present study, high speed camera, programmable power supply and acquisition of thermocouple reading are synchronized by workstation. This ensures the physical identification of the exact

moment of ONB and its corresponding measured temperature can be assured through the common platform of LABVIEW program. During quasi-steady heat supply, two different incidents are identified immediately after ONB as shown in Fig. 10. ONB is observed in the beginning which is followed by the onset of boiling driven (OBD) phase. ONB and OBD are observed by the high speed camera. The sudden rise in the heat flux from the surface is noticed as number of bubble considerably increased at OBD. At quasi-steady heat supply, the stored energy in the sample drops due to OBD heat transfer which results in sharp fluctuation in the measured temperature immediately after OBD. This moment at which surface temperature drops is called as overshoot
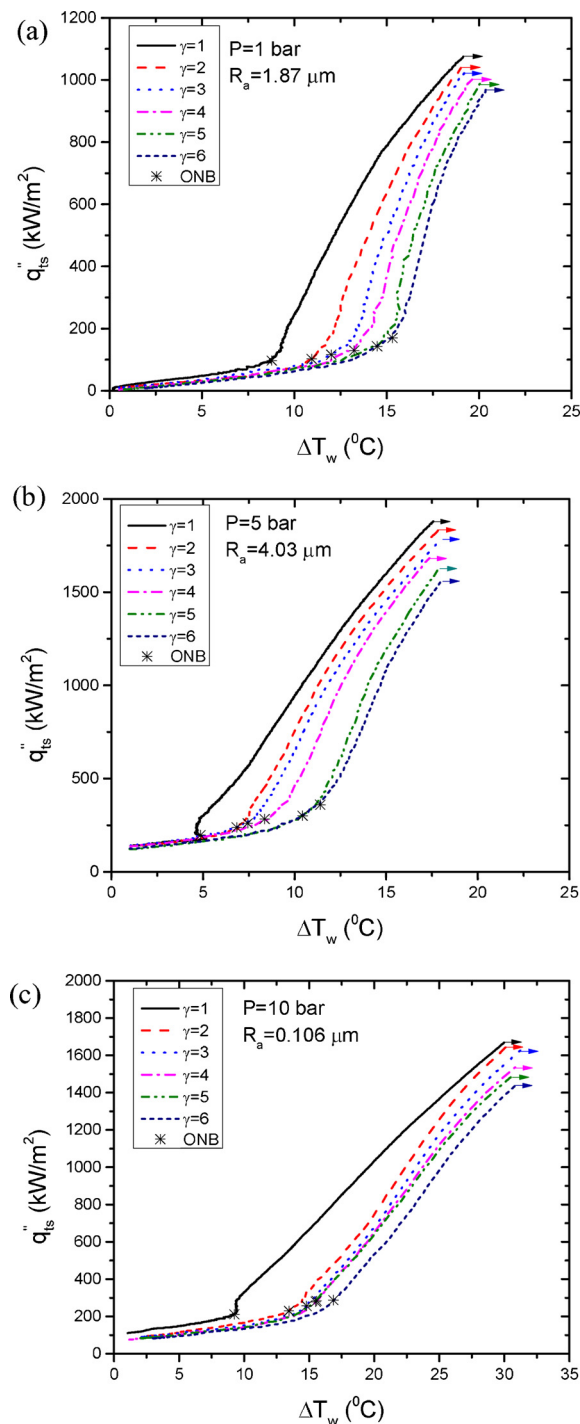

Fig. 8. Boiling curves of the sample (a) P = 1 bar, $R_a = 1.87\,\mu m$ (b) P = 5 bar, $R_a = 4.03\,\mu m$ (c) P = 10 bar, $R_a = 0.106\,\mu m$ at different γ.
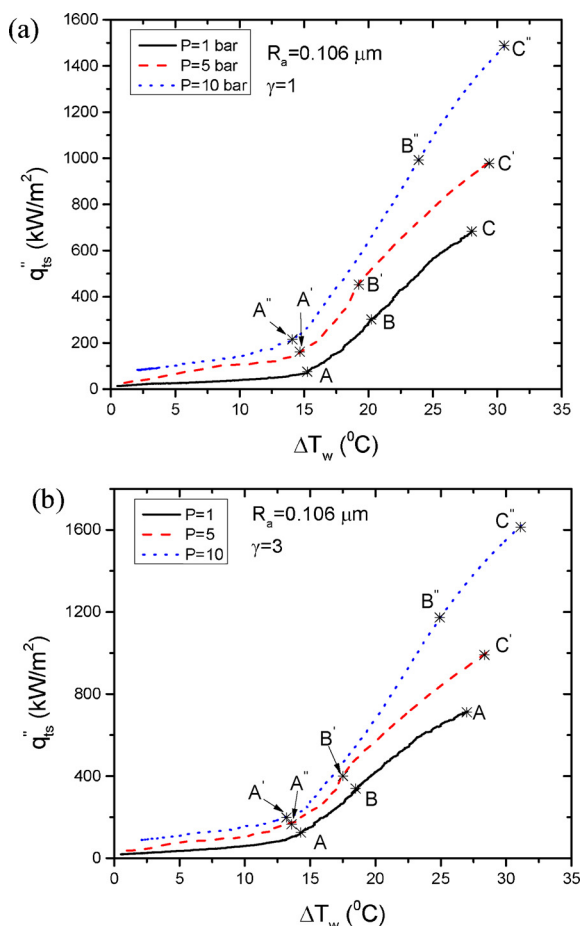
Fig. 9. Boiling curves of the sample $R_a = 0.106\,\mu\text{m}$ at time constant (a) $\gamma = 1$ (b) $\gamma = 3$ at different pressures.
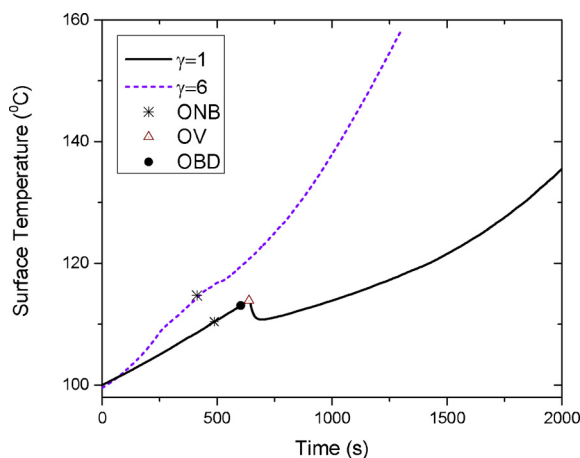

Fig. 10. Time trace of the surface temperature at P = 1 bar.

Fig. 11. Variation in non-dimensional h_{ts} with non-dimensional q_{ts} for different surface roughness at (a) P = 1 bar, $\gamma = 3$ (b) P = 5 bar, $\gamma = 5$ (c) P = 10 bar, $\gamma = 2$.

(OV) temperature. The ONB and OBD points coincide during the rapid transient as the explosive bubble growth is observed at the ONB. The absence of OV temperature indicates that the heat removed after ONB is not enough to reduce the rapidly increasing surface temperature.

3.6. Variation in transient HTC with transient heat flux

Non-dimensional h_{ts} and q_{ts} is derived from the reference values of h and q suggested by Kim et al. [19] as given in Eq. (4). The values h_0 and q_0'' are calculated from the thermo-physical properties of the saturated
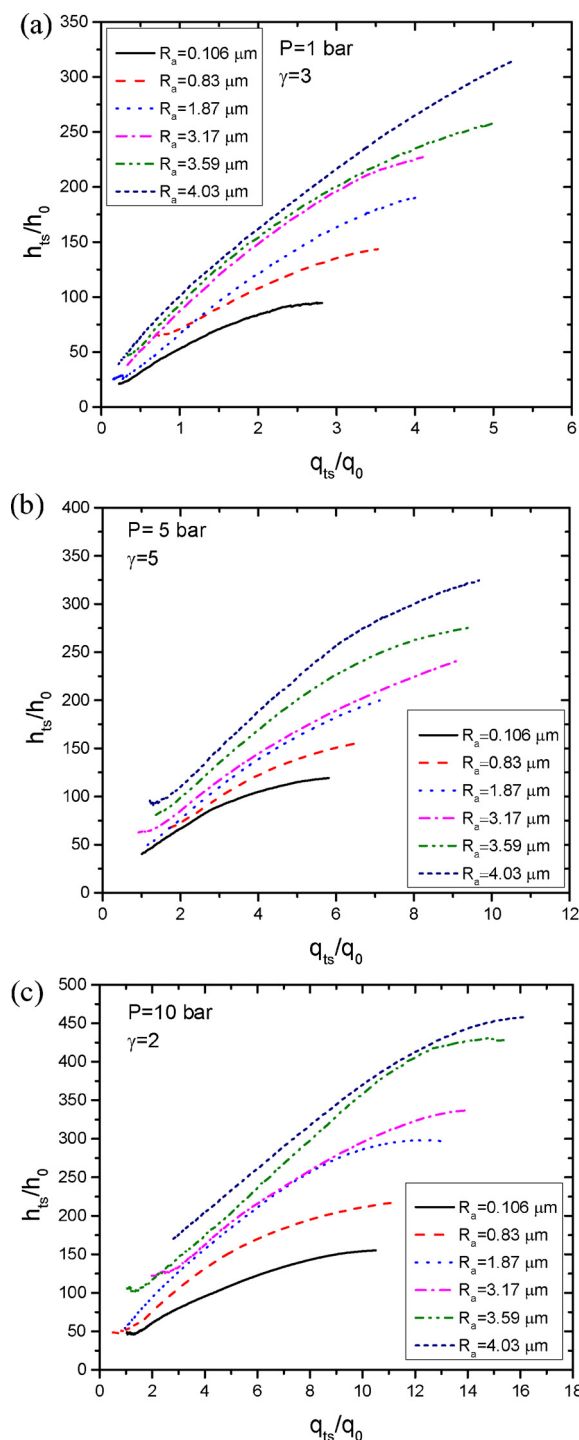
liquid at reference condition of 1 bar, 5 bar and 10 bar pressure. Variation in non-dimensional h_{ts} with non-dimensional q_{ts} at each pressure for different R_a is shown in Fig. 11. The curves shift upward gradually with increase in the surface roughness at each pressure. The identical trend of the curves is observed for each time constant of exponential heat supply. It suggests the augmentation of HTC due to increase in the R_a and pressure.

$$h_0 = \frac{\mu_l c_{pl}}{P \eta_l}\left[\frac{g(\rho_l - \rho_v)}{\sigma}\right]^{1/2}; \quad q_0'' = \mu_l h_{fg}\left[\frac{g(\rho_l - \rho_v)}{\sigma}\right]^{1/2} \quad (4)$$

3.7. Critical heat flux

The transition from FDNB to film boiling occurs due to formation of vapor blanket on the entire surface. The upper limit of the heat flux at this moment is defined as CHF. The peak of the curve shown in Fig. 11 that corresponds to the maximum HTC is identified as CHF. After CHF, the HTC decreases with the increase in the wall superheat. Though the present study is focused on transient pool boiling heat transfer, the steady state pool boiling study is also carried to examine the effect of heating condition on CHF. The steady state CHF values for different R_a are plotted in Fig. 12 at 1 bar, 5 bar and 10 bar. The transient CHF of different samples at the time constant $\gamma = 1$ and $\gamma = 6$ is also plotted in Fig. 12 at different R_a for comparison. It is found that both, steady and transient CHF increase with increase in the R_a as well as with increase in the pressure. The comparative study suggests that transient CHF is lower than that of the steady state CHF for each sample.

The mechanism of liquid-vapor interaction plays vital role in the occurrence of CHF. The rapid unsteady state heat supply causes the instability in the liquid replenishment. The thickness of superheated liquid layer increases in the same order as that of heat supply resulting in drop in the surface tension forces on the bubble meniscus. At this dynamic phase, bubble rapidly spreads over the horizontal surface causing large bubble to depart from the surface.

The transient CHF for $R_a = 4.03\,\mu m$ at heat supply of $\gamma = 1$ and $\gamma = 6$ is found to be 9.38% and 24.60%, respectively, lower than the corresponding steady-state CHF at P = 1 bar. The transient CHF for $R_a = 4.03\,\mu m$ at $\gamma = 6$ is found to be 31.60% lower than the corresponding steady-state CHF at P = 10 bar. It is found that transient CHF of $R_a = 4.03\,\mu m$ during exponential transient of $\gamma = 1$ is higher than the steady state CHF of $R_a = 0.106\,\mu m$. Hence, conclusion may be drawn that drop in the CHF due to unsteady heat supply of $\gamma = 1$ can be compensated by making the surface rough. This can be explained by bubble dynamics and wettability study. As discussed earlier, though it is vague to characterize surface solely based on R_a, it is the most suitable parameter related to the unidirectional scratches, where R_a relates to the radius of the capillary tube. Additional parameter S_m is also quantified to explain the role of unidirectional scratches in CHF enhancement. It is observed during characterization that mean spacing S_m between two adjacent scratches increases with increase in R_a. It is thus complex phenomena to justify the CHF enhancement. Hydrophilicity of the rough surface and the quantity of liquid supply through the scratches increase with increase in R_a. The increase in S_m resulted in the increase in spacing between the nucleated bubbles. Thus horizontal bubble coalescence is retarded at high heat flux. Increased distance between two adjacent bubbles also triggered the induced liquid supply from the peak of scratch. Thus the combined effect of R_a and S_m resulted in CHF enhancement. Increase in the time constant γ has remarkably reduced the transient CHF and it is found that drop in the CHF during short transient ($\gamma = 6$) can be compensated only at P = 1 bar and P = 5 bar by increasing the surface roughness upto 4.03 μm. The variation in CHF at P = 5 bar with R_a at different time constant γ is shown in Fig. 13. Marginal drop in the transient CHF is noticed due to increase in the γ. At P = 5 bar, 2.56% and 16.95% drop in the CHF for $R_a = 4.03\,\mu m$ is found due to increase in the γ from 1 to 6, respectively. It is found that the transient CHF for $R_a = 0.106\,\mu m$ increases by 40.21% and 128.66% due to increase in the pressure to P = 5 bar and 10 bar, respectively.

The variation in CHF with γ at P = 10 bar is shown in Fig. 14. It is found that transient CHF gradually decreased with increase in the γ of exponential heat supply. The CHF values for the sample $R_a = 4.03\,\mu m$ dropped close to the CHF value for $R_a = 3.59\,\mu m$ which justifies the

inefficient heat removal from the surface during rapid exponential heating. It is clear that nucleation site density increases with increase in R_a and surface temperature. The rapid heat supply to the sample of $R_a = 4.03\,\mu m$ at $\gamma = 6$ can trigger the number of bubbles by multifold which leads to horizontal bubble coalescence. This mechanism of boiling at rapid heating suggests the upper limit of the R_a which removes the heat efficiently during transient heat supply.

3.8. Transient maximum heat transfer coefficient

Transient maximum heat transfer coefficient ($h_{max,ts}$) obtained for each sample at different pressure and heat supply of different time constant is presented in Fig. 15. It is found that $h_{max,ts}$ considerably increased with increase in R_a signifying the efficient heat removal during each transient heat supply due to improved surface roughness values. The time constant during exponential heat supply has adverse effect on $h_{max,ts}$ however it is found to be moderate. The percentage increase in $h_{max,ts}$ increases with increase in the pressure at fixed R_a.

4. CHF and HTC correlation

In this investigation, it is found that transient CHF decreases with increase in the time constant and CHF of steady state condition is found to be higher than transient CHF for each sample. It is important to develop a relation between steady and transient CHF to predict the drop in CHF due to transient heat supply. A correlation for steady state CHF as a function of R_a and P is derived as given in Eq. (5) by least square regression analysis. It illustrates that the influence of R_a and P on CHF diminishes at relatively high value. The predicted $q_{CHF,ss}''$ and experimental $q_{CHF,ss}''$ are compared and it is found that present correlation predicts $q_{CHF,ss}''$ with MAE of 6.05%. The correlation of $q_{CHF,ts}''$, as given in Eq. (6), is also developed by similar method and the comparison between predicted $q_{CHF,ts}''$ and experimental $q_{CHF,ts}''$ is given in Fig. 16. This correlation predicts $q_{CHF,ts}''$ with MAE of 10.11%.

$$q_{CHF,ss}'' = 1280.8\,(R_a)^{0.14}(P)^{0.27} \quad (5)$$

$$q_{CHF,ts}'' = 1031.9\,(\gamma)^{-0.08}(R_a)^{0.14}(P)^{0.27} \quad (6)$$

A relation between steady and transient CHF is derived using Eqs. (5) and (6) and is expressed in Eq. (7).

$$q_{CHF,ts}'' = 0.81\,(\gamma)^{-0.08} q_{CHF,ss}'' \quad (7)$$

Many investigators have suggested that HTC is a strong function of surface roughness and correlations in the form of $h \propto C R_a^m q^n$ are
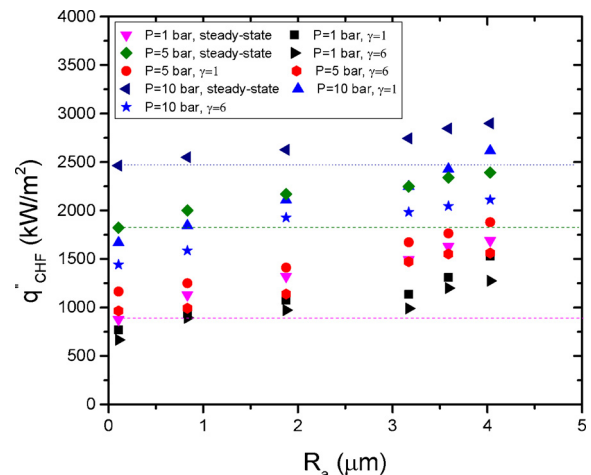

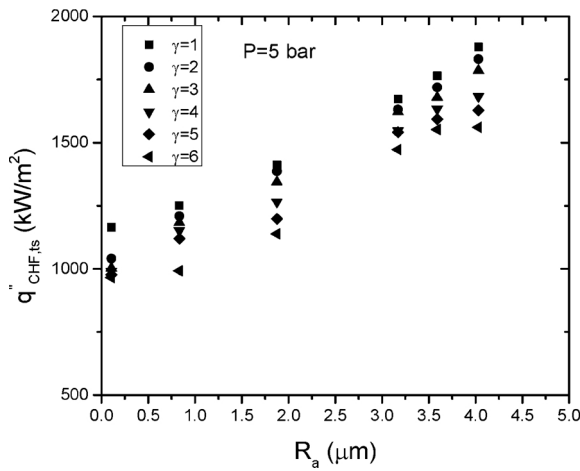**Fig. 12.** Effect of surface roughness on steady and transient CHF at various pressures.

Fig. 13. Effect of surface roughness on transient CHF at different time constant (γ).
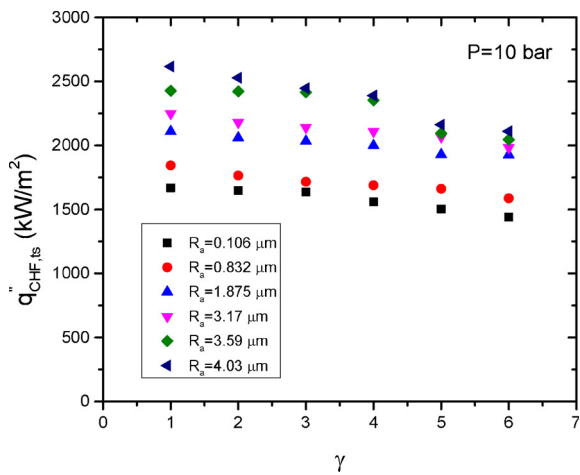

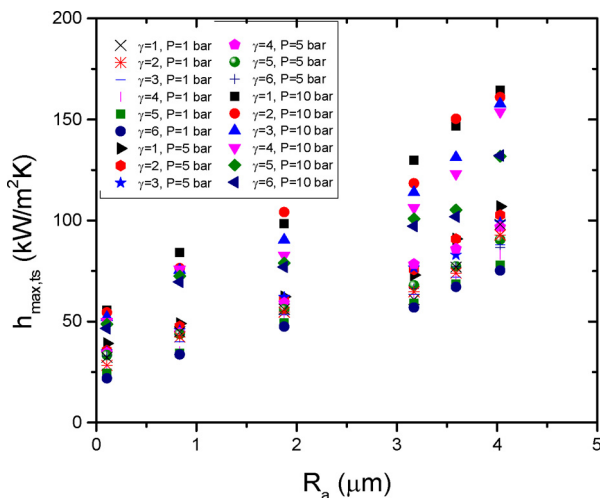**Fig. 14.** Effect of time constant on transient CHF at different surface roughness.

Fig. 15. Effect of surface roughness on transient HTC at different time constant and pressure.

proposed. The correlation presented by Gorenflo [20] is found to be useful, as it predicts the HTC of almost all the fluids at high pressure. Gorenflo [20] used the exponent of R_a, $m = 0.133$ as suggested by Stephan [21]. A simplified form of Gorenflo correlation is given in Eq. (8).
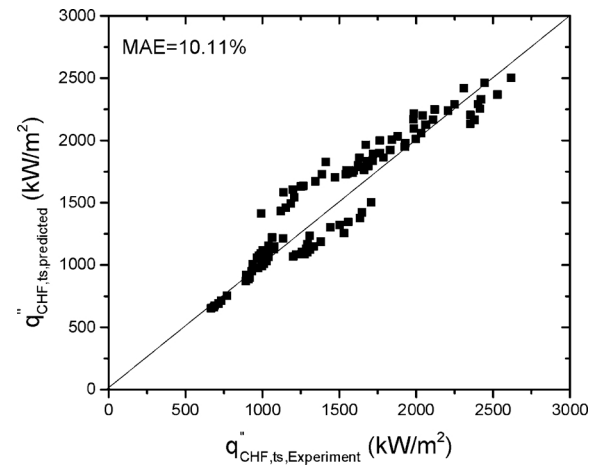

Fig. 16. Comparison of predicted CHF by Eq. (6) with the experimental CHF at exponential heat supply.

$$h = h^{'} \times F_P \times F_q \times F_R \qquad (8)$$

where,

$$F_P = 1.73P_r^{0.27} + \left(6.1 + \frac{0.68}{1-P_r}\right)P_r^2; \quad F_q = \left(\frac{q}{q^{'}}\right)^n; \quad n = 0.9 - 0.3P_r^{0.15}; \quad F_R$$

$$= \left(\frac{R_a}{R_{a0}}\right)^{0.133}$$

The reference conditions for pure water are $h^{'} = 5600 \, \text{W/m}^2\text{K}$, $q^{'} = 20,000 \, \text{W/m}^2$ and $R_{aO} = 0.4 \, \mu\text{m}$. The values of predicted HTC by Eq. (8) are compared with experimental values and it is found that error between the experimental transient HTC and predicted HTC increases with increase in the time constant γ. In present study it is found that HTC is also the function of γ. As Eq. (8) does not consider the effect of γ for the prediction of HTC, it is found that predicted HTC values are higher than the experimental values. The MAE between predicted and experimental HTC is 20.96%. Hence the Gorenflo correlation is modified to account for the effect of transient heat supply wherein the time constant γ is incorporated. γ can be called as non-dimensional time value which justifies the rate of transient i.e. slow, intermediate or rapid transient. Thus, modified Gorenflo correlation is formulated as given in Eq. (9).

$$h_{ts} = h^{'} \times F_P \times F_q \times F_R \times F_\gamma \qquad (9)$$

where, $F_\gamma = \gamma^s = \left(\frac{t}{\tau}\right)^s$

Following the Gorenflo's work, the exponent of the time constant is obtained from the regression analysis. The predicted HTC values are plotted at corresponding experimental values as shown in Fig. 17. It is found that MAE between the experimental and predicted HTC is 14.91% at $s = -0.15$. The negative value of s justifies the inverse relation between HTC and γ. HTC considerably drops with increase in γ due to its adverse effect on bubble mechanism. This mechanism is discussed in the earlier section.

5. CHF model

Critical heat flux is the maximum limit of efficient heat removal from the surface and hence it is vital to predict the CHF through the knowledge of governing mechanism. Several approaches have been proposed earlier which can be broadly classified as far-field and near field model. Zuber [22] proposed the hydrodynamic instability model considering the far-field effect wherein it was assumed that CHF occurs because of Helmholtz instability. At the point of CHF, Helmholtz instability of the departing bubble becomes unstable which results in the failure of the surface-fluid interaction. Lienhard and Dhir [23] modified
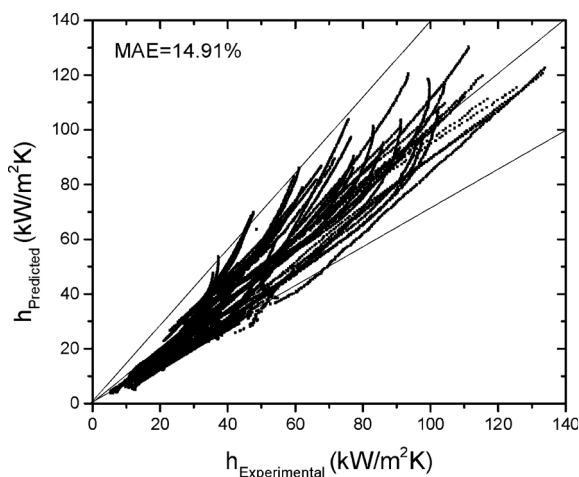
Fig. 17. Comparison of predicted transient HTC by Eq. (9) with the experimental HTC.

Zuber's model by considering the dominance of Taylor wavelength at CHF. These approaches do not consider the role of surface characteristics in the occurrence of CHF. Moreover, the effect of contact angle and surface forces are not considered in their model. Macrolayer evaporation model so called near field approach was proposed by Haramura and Katto [24]. This model assumes the bubble growth over the macrolayer and at complete dry-out condition of the macrolayer leads to the CHF. Zhao et al. [25,26] developed the CHF model for steady and transient heating condition. They estimated the time variant microlayer thickness and its evaporation during each bubble cycle. A complete evaporation of microlayer thickness is considered as a liquid dry-out which results in the CHF. Recently, researchers proposed the hydrodynamic model coupled with surface-fluid characteristics like contact angle [27,28], surface roughness [19,29–31], heater size [32], nucleation site density [33], capillary wicking [34] and heater orientation [35]. Most widely accepted CHF model proposed by Kandlikar [28] is based on force balance approach. The CHF is identified by balancing the forces acting on the bubble parallel to the upward facing boiling surface. It is considered that at CHF, bubble spreads over the surface resulting in the formation of vapor blanket. Ahn et al. [34] claimed the key role of wetting property and liquid spreading due to capillary wicking of the surface in the CHF enhancement. Separate term of capillary wicking was included in the model to estimate CHF. Quan et al. [36] developed CHF model for micro/nanostructures based on force balance analysis, considering the effects of contact angle, capillary wicking force and roughness factor r. Li and Huang [31] recently proposed CHF model for the surfaces of micro roughness which includes micro-pillar, micro-ridge structures as well as random roughness made by emery paper. The CHF enhancement was accounted by considering separate term in the Kandlikar's model. This term signifies heat flux due to evaporation of the capillarity-induced liquid supply. Kim et al. [19] considered the effect of roughness due to unidirectional scratches on the contact angle and the same is incorporated in the Kandlikar's

model. They assumed that each unidirectional scratch acts as a capillary tube and thus relates the surface roughness with the capillary tube radius. Additional force due to capillary action through the scratches is estimated as a function of surface roughness. Thus CHF enhancement due to increase in the surface roughness is predicted by the proposed model.

5.1. Present model

It is proved by the earlier study that CHF enhancement due to improved surface characteristics like micro-pillar structure, surface roughness, surface wettability and nucleation site density can be modelled by force balance approach. As R_a solely can not characterize the surface, additional parameter i.e. spacing between two adjacent scratches (S_m) is also considered in the present model. Static contact angle between water droplet and the surface before the pool boiling experiments is considered in the literature. The parameter, so called bubble angle (Θ_b), is the angle between the bubble meniscus, surface and the surrounding liquid seems to be the most relevant and real time entity to be considered instead of contact angle of the water droplet. Phan et al. [37–39], Teodori et al. [40] and Malavasi et al. [41] suggested a relation between static angle and bubble angle. The trend of bubble departure diameter and contact angle was also presented. They developed a model where the concept of macro- and micro-contact angles is coined. In the present study, the bubble angle for four discrete bubbles at each pressure and roughness value is measured. Schematic diagram of bubble angle measurement is shown in Fig. 18. The average value of bubble angle at different pressures is given in Fig. 19. It is found that contact angle of the water droplet measured at 25 °C is approximately 9° higher than the bubble angle measured at saturated condition. This bubble angle study suggests that surface becomes hydrophilic with increase in R_a. However influence of R_a on bubble contact angle diminishes at high pressure.

Present study thus includes the effect of surface roughness on bubble angle at different pressures which is not yet considered in the CHF model presented in the literature. Present experimental study of transient pool boiling is carried out at high pressure of distilled water using samples of different surface roughness value. The time constant (γ) should be included separately in the CHF model to predict transient CHF. The forces acting on the bubble parallel to the surface, as shown in Fig. 20, are considered in the present force balance approach. Bubble experiences a pull force F_M during unsteady growth due to momentum change which allows bubble to spread over the surface. Simultaneously, sum of drag forces like surface tension force, gravity and capillary force also acts on the bubble which retains its original position and does not allow its horizontal growth. Visualization study suggests that fully developed nucleate boiling regime turns into film boiling due to progressive horizontal bubble coalescence. This phase transition occurs when F_M surpasses the sum of drag forces resulting in CHF which is upper limit of efficient heat removal from the surface.

CHF is identified by the force balance as given in Eq. (12).

$$F_M = F_{s,t} + F_{s,b} + F_g + F_c \tag{12}$$

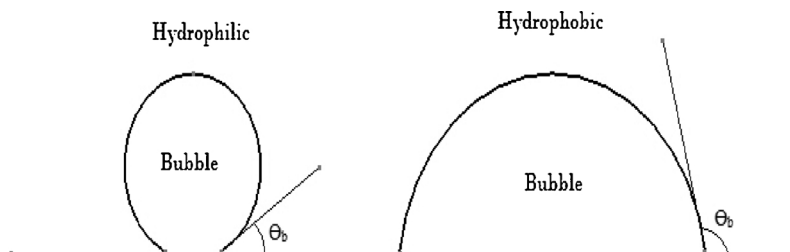A growing bubble experiences a force on its meniscus due to the

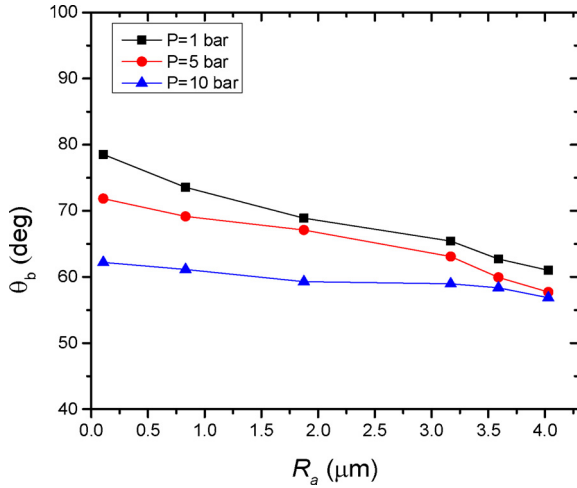**Fig. 18.** Schematic representation of bubble angle measurement.

Fig. 19. Variation in bubble angle with R_a at different pressure.

change in momentum caused by the increase in velocity. F_M is the momentum change due to evaporation of the liquid and can be expressed as given in Eq. (13).

$$F_M = \frac{1}{\rho_v}\left(\frac{q_l''}{h_{fg}}\right)^2 H_b \tag{13}$$

$F_{s,t}$ and $F_{s,b}$, given in Eq. (14), are the surface tension forces acting at top and bottom of the bubble, respectively.

$$F_{s,t} = \sigma, \ F_{s,b} = \sigma\cos\theta_b \tag{14}$$

F_g refers to the gravity force which is formulated in Eq. (15) for the horizontal upward facing surface.

$$F_g = \frac{1}{2}g(\rho_l - \rho_v)H_b^2 \tag{15}$$

H_b is the equivalent height of the bubble and it is obtained by Eq. (16). Bubble diameter can be formulated, as given in Eq. (17), from Taylor unstable wavelength, as suggested by Kandlikar [28].

$$H_b = \frac{D_b}{2}(1 + \cos\theta_b) \tag{16}$$

$$D_b = \frac{\lambda_T}{2} = \pi\left[\frac{\sigma}{g(\rho_l - \rho_v)}\right]^{1/2} \tag{17}$$

The capillary pressure P_c which acts on the bubble through the small tube of radius R_c is derived by Young-Laplace equation, as given in Eq. (18).

$$P_c = \frac{2\sigma\cos\theta_b}{R_c} \tag{18}$$

Each unidirectional scratch on the surface is assumed as a single capillary tube and many such tubes lie underneath the bubble.

Considering this assumption, it can be expressed, as given in Eq. (19), that the radius of the capillary tube is proportional to the roughness value R_a.

$$R_a \propto R_c \tag{19}$$

Capillary force expressed by Eq. (20) considers the number of capillary tubes underneath the bubble, radius of each tube and the capillary pressure inside each tube.

$$F_c = N\pi R_c^2 P_c = N\pi R_c^2 \frac{2\sigma\cos\theta_b}{R_c} = 2\pi N R_c \sigma\cos\theta_b \tag{20}$$

Kim et al. [19] expressed the capillary force, as given in Eq. (21), by considering inverse proportion between N and S_m.

$$F_c = 2\pi C\left(\frac{R_a}{S_m}\right)\sigma\cos\theta_b \tag{21}$$

Combining all the above forces, force balance is expressed by Eq. (22).

$$\frac{1}{\rho_v}\left(\frac{q_l''}{h_{fg}}\right)^2 H_b = \sigma + \sigma\cos\theta_b + \frac{1}{2}g(\rho_l - \rho_v)H_b^2 + 2\pi C\left(\frac{R_a}{S_m}\right)\sigma\cos\theta_b \tag{22}$$

Eq. (23) is obtained by rearranging the above equation to express q_l''

$$q_l'' = h_{fg}\rho_v^{0.5}\left[\sigma g(\rho_l - \rho_v)\right]^{0.25}\left[\frac{2}{\pi} + \frac{\pi}{4}(1 + \cos\theta_b) + \frac{4C\cos\theta_b}{1 + \cos\theta_b}\left(\frac{R_a}{S_m}\right)\right]^{0.5} \tag{23}$$

Steady-state CHF can be obtained by the Eq. (24) as suggested by Kandlikar [28].

$$q_{CHF,ss}'' = \left(\frac{1 + \cos\theta_b}{16}\right)q_l'' \tag{24}$$

The final form of transient CHF model of the samples with wide range of surface roughness R_a under exponential heat supply ranging from $\gamma = 1$ to $\gamma = 6$ at pressure upto 10 bar is obtained by combining Eqs. (7), (23) and (24) and is given in Eq. (25).

$$q_{CHF,ts}'' = \left(\frac{0.81}{\gamma^{0.08}}\right)\left(\frac{1 + \cos\theta_b}{16}\right)\{h_{fg}\rho_v^{0.5}\left[\sigma g(\rho_l - \rho_v)\right]^{0.25}\} \\ \left[\frac{2}{\pi} + \frac{\pi}{4}(1 + \cos\theta_b) + \frac{4C\cos\theta_b}{1 + \cos\theta_b}\left(\frac{R_a}{S_m}\right)\right]^{0.5} \tag{25}$$

The proportionality constant C determines the number of tubes underneath the growing bubble. As the bubble base diameter decreases with increase in pressure, the value of C decreases with increase in the pressure. It is obtained from Eq. (25) using θ_b, R_a, S_m, and CHF. The transient CHF obtained by Eq. (25) is compared with present experimental data and presented in Fig. 21. The predicted transient CHF is found to be in good agreement with the experimental transient CHF with MAE of 11.89%. Thus new term viz. time constant (γ) and bubble angle (θ_b) are included in the transient CHF model wherein roughness
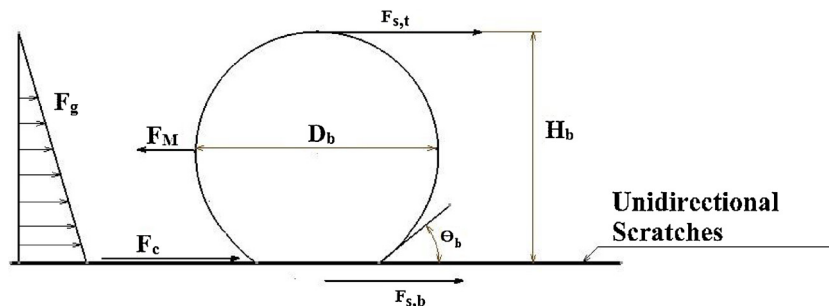

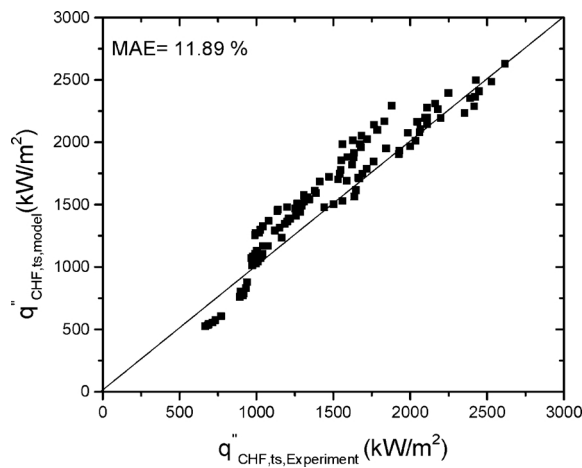**Fig. 20.** Forces acting on the bubble parallel to the surface.

Fig. 21. Comparison of experimental and predicted CHF.

parameter R_a and S_m is also considered.

6. Conclusion

The pool boiling experiments were conducted on the samples of wide range of R_a varying from 0.106 μm to 4.03 μm in saturated water at pressures 1 bar, 5 bar and 10 bar at different rate of exponential heat supply. Effect of R_a and γ on transient CHF was extensively examined at various pressures. Transition of boiling phase at different time constant of exponential heat supply was observed by high speed camera. Following conclusions are deduced from the present study.

- HSN is observed during initial phase of the boiling i.e. before FDNB regime whereas CHF during exponential heat supply occurred due to hydrodynamic instability.
- Steady-state CHF is found to be higher than the transient CHF for all the samples. Steady-state CHF for $R_a = 0.106$ μm at P = 10 bar is found to be 41.48% higher than the corresponding transient CHF during $\gamma = 6$.
- Considerable increase in the transient CHF is noticed with increase in R_a and P whereas it gradually decreases with increase in γ.
- Compound effect of R_a and S_m resulted in the CHF enhancement which can be justified by improved capillary wicking and increased number of nucleation sites. Transient CHF enhancement for $R_a = 3.59$ μm at $\gamma = 1$ is found to be 69.87%, 65.76% and 43.19% at pressure P = 1 bar, P = 5 bar and P = 10 bar, respectively.
- The transient CHF for $R_a = 3.17$ μm at P = 5 bar and P = 10 bar during exponential heat supply of $\gamma = 3$ increased by 32.13% and 91.48%, respectively, from that of at P = 1 bar.
- Transient CHF decreased gradually with increase in γ. At P = 10 bar, the transient CHF for the sample of $R_a = 1.87$ μm is found to be decreased by 9.12% due to increase in the γ from 1 to 6, respectively.
- Modified Gorenflo correlation, which includes the non-dimensional time constant γ, predicts the present transient HTC values with MAE of 14.91%.
- CHF model based on force balance approach is developed incorporating the effect of R_a, S_m, time constant γ and bubble angle. The present model predicts the transient CHF with MAE of 11.89%.

References

[1] M.W. Rosenthal, An experimental study of transient boiling, Nucl. Sci. Eng. 2 (1957) 640–656.
[2] H.A. Johnson, Transient boiling heat transfer to water, Int. J. Heat Mass Transf. 14 (1971) 67–82.
[3] A. Sakurai, M. Shiotsu, K. Hata, Boiling heat transfer characteristics for heat inputs with various increasing rates in liquid nitrogen, Cryogenics 32 (5) (1992) 421–428.
[4] Sakurai and Shiotsu, Transient pool boiling heat transfer part 1: incipient boiling superheat, J. Heat Transf. 99 (1977) 547–553.
[5] Sakurai and Shiotsu, Transient pool boiling heat transfer part 2: boiling heat transfer and Burnout, J. Heat Transf. 99 (1977) 554–560.
[6] V.I. Deev, V.S. Htay Lwin Oo, K.V. Kharitonov, A.A. Kutsenko, Lavrukhin, Critical heat flux modeling in water pool boiling during power transients, Int. J. Heat Mass Transf. 50 (2007) 3780–3787.
[7] Marie-Christine Duluc, Benoit Stutz, Monique Lallemand, Transient nucleate boiling under stepwise heat generation for highly wetting fluids, Int. J. Heat Mass Transf. 47 (2004) 5541–5553.
[8] Guan-Yu Su, Matteo Bucci, Thomas McKrell, Jacopo Buongiorno, Transient boiling of water under exponentially escalating heat inputs. Part I: pool boiling, Int. J. Heat Mass Transf. 96 (2016) 667–684.
[9] B.V. Balakin, M.I. Delov, D.M. Kuzmenkov, K.V. Kutsenko, A.A. Lavrukhin, A.S. Marchenko, Boiling crisis in cryogenic fluids during unsteady heat supply, Int. J. Heat Mass Transf. 111 (2017) 1107–1111.
[10] V. Drach, N. Sack, J. Fricke, Transient heat transfer from surfaces of defined roughness into liquid nitrogen, Int. J. Heat Mass Transf. 39 (9) (1996) 1953–1961.
[11] K. Fukuda, M. Shiotsu, Sakurai, Effect of surface conditions on transient critical heat fluxes for a horizontal cylinder in a pool of water at pressures due to exponentially increasing heat inputs, Nucl. Eng. Des. 200 (2000) 55–68.
[12] Jongdoc Park, Katsuya Fukuda, Qiusheng Liu, CHF phenomena by photographic study of boiling behavior due to transient heat input science and technology of nuclear installations, Sci. Technol. Nucl. Install. (2012) 1–12.
[13] Min Han Htet, Katsuya Fukuda, Qiusheng Liu, Transient boiling critical heat flux on horizontal vertically oriented ribbon heater with treated surface condition in pool of water, Mech. Eng. J. 3 (3) (2016) 1–19.
[14] Shuai Gong, Ping Cheng, Direct numerical simulations of pool boiling curves including heater's thermal responses and the effect of vapor phase's thermal conductivity, Int. Commun. Heat Mass Transf. 87 (2017) 61–71.
[15] J. McHale, S. Garimella, Bubble nucleation characteristics in pool boiling of a wetting liquid on smooth and rough surfaces, Int. J. Multiph. Flow 36 (6) (2010) 249–260.
[16] B. Bourdon, R. Rioboo, Marengo, E. Gosselin, J. de Coninck, Influence of the wettability on the boiling onset, Langmuir 28 (2012) 1618–1624.
[17] Avdhoot Walunj, A. Sathyabhama, Comparative study of pool boiling heat transfer from various microchannel geometries, Appl. Therm. Eng. 128 (2017) 672–683.
[18] A. Sakurai, M. Shiotsu, K. Hata, K. Fukuda, Photographic study on transitions from non-boiling and nucleate boiling regime to film boiling due to increasing heat inputs in liquid nitrogen and water, Nucl. Eng. Des. 200 (2000) 39–54.
[19] J. Kim, S. Jun, R. Laksnarain, S.M. You, Effect of surface roughness on pool boiling heat transfer at a heated surface having moderate wettability, Int. J. Heat Mass Transf. 101 (2016) 992–1002.
[20] D. Gorenflo, Pool Boiling, VDI Heat Atlas, VDI Verlag, Düsseldorf, 1993.
[21] K. Stephan, Mechanismus und Modellgesetz des Wärmeübergangs bei der Blasenverdampfung, Chemie-Ingenieur-Technik 35 (11) (1963) 775–784.
[22] N. Zuber, On the stability of boiling heat transfer, Trans. ASME J. Heat Transf. 8 (3) (1958) 711–720.
[23] J.H. Lienhard, V.K. Dhir, Hydrodynamic Theory of the Peak and Minimum Pool Boiling Heat Fluxes, CR-2270, (1973).
[24] Y. Haramura, Y. Katto, A new hydrodynamic model of critical heat flux, applicable widely to both pool and forced convection boiling on submerged bodies in saturated liquids, Int. J. Heat Mass Transf. 26 (1983) 389–399.
[25] Y.H. Zhao, T. Masuoka, T. Tsuruta, Unified theoretical prediction of fully developed nucleate boiling and critical heat flux based on a dynamic micro layer model, Int. J. Heat Mass Transf. 45 (2002) 3189–3197.
[26] Y.H. Zhao, T. Masuoka, T. Tsuruta, Theoretical studies on transient pool boiling based on microlayer model, Int. J. Heat Mass Transf. 45 (2002) 4325–4331.
[27] Yu.A. Kirishenko, P.S. Cherniakov, Determination of the first critical thermal heat flux on flat heaters, J. Eng. Phys. 20 (1973) 699–702.
[28] S.G. Kandlikar, A theoretical model to predict pool boiling CHF incorporating effects of contact angle and orientation, J. Heat Transf. 123 (2001) 1071–1079.
[29] J.J. Wei, H. Honda, Effects of fin geometry on boiling heat transfer from silicon chips with micro-pin-fins immersed in FC-72, Int. J. Heat Mass Transf. 46 (2003) 4059–4070.
[30] J.Y. Jung, H.Y. Kwak, Effect of surface condition on boiling heat transfer from silicon chip with submicron-scale roughness, Int. J. Heat Mass Transf. 49 (2006) 4543–4551.
[31] Ran Li, Zhongwei Huang, A new CHF model for enhanced pool boiling heat transfer on surfaces with micro-scale roughness, Int. J. Heat Mass Transf. 109 (2017) 1084–1093.
[32] K.N. Rainey, S.M. You, Effects of heater size and orientation on pool boiling heat transfer from microporous coated surfaces, Int. J. Heat Mass Transf. 44 (2001) 2589–2599.
[33] Ming-Chang Lu, Chih-Hung Huang, Chung-Te Huang, Yu-Chi Chen, A modified hydrodynamic model for pool boiling CHF considering the effects of heater size and nucleation site density, Int. J. Therm. Sci. 91 (2015) 133–141.
[34] H.S. Ahn, H.J. Jo, S.H. Kang, M.H. Kim, Effect of liquid spreading due to nano/microstructures on the critical heat flux during pool boiling, Appl. Phys. Lett. 98 (2011) 071908.
[35] A.H. Howard, I. Mudawar, Orientation effects on pool boiling critical heat flux (CHF) and modeling of CHF for near-vertical surfaces, Int. J. Heat Mass Transf. 42 (1999) 1665–1688.
[36] X. Quan, L. Dong, P. Cheng, A CHF model for saturated pool boiling on a heated surface with micro/nano-scale structures, Int. J. Heat Mass Transf. 76 (2014) 452–458.

[37] H. Phan, N. Caney, P. Marty, J. Colasson, Surface wettability control by nano-coating: The effects on pool boiling heat transfer and nucleation mechanism, Int. J. Heat Mass Transf. 52 (2009) 5459–5471.

[38] H. Phan, N. Caney, P. Marty, S. Colasson, J. Gavillet, A model to predict the effect of contact angle on the bubble departure diameter during heterogeneous boiling, Int. Commun. Heat Mass Transf. 37 (2010) 964–969.

[39] H.T. Phan, R. Bertossi, N. Caney, P. Marty, J. Colasson, A model to predict the effect of surface wettability on critical heat flux, Int. Commun. Heat Mass Transf. 39 (2012) 1500–1504.

[40] E. Teodori, T. Valente, I. Malavasi, A.S. Moita, M. Marengo, A.L.N. Moreira, Effect of extreme wetting scenarios on pool boiling conditions, Appl. Therm. Eng. 115 (2017) 1424–1437.

[41] I. Malavasi, E. Teodori, A.S. Moita, A.L.N. Moreira, M. Marengo, Wettability effect on pool boiling: a review, in: J. Thome (Ed.), Encyclopaedia of Two-Phase Heat Transfer and Flow III: Macro and Micro Flow Boiling and Numerical Modeling Fundamentals (A 4-volume Set), vol. 4, World Scientific Publishing Co Pte Ltd., 2018ISBN: 978-981-3227-31-6.